High-order harmonic generation from arbitrarily oriented diatomic molecules including nuclear motion and field-free alignment

C. B. Madsen and L. B. Madsen
Department of Physics and Astronomy, University of Aarhus, 8000 Århus C, Denmark
(Received 27 April 2006; published 3 August 2006)

We present a theoretical model of high-harmonic generation from diatomic molecules. The theory includes effects of alignment as well as nuclear motion and is used to predict results for N_2, O_2, H_2, and D_2. The results show that the alignment dependence of high-harmonics is governed by the symmetry of the highest occupied molecular orbital and that the inclusion of the nuclear motion in the theoretical description generally reduces the intensity of the harmonic radiation. We compare our model with experimental results on N_2 and O_2, and obtain very good agreement.

DOI: 10.1103/PhysRevA.74.023403 PACS number(s): 33.80.Rv, 42.65.Ky, 33.15.Mt

I. INTRODUCTION

High-harmonic generation (HHG) is a process in strong-field physics that occurs when the nonperturbative driving of an electron by an external field makes it leave its parent atom or molecule, propagate in the field, and finally when the electron is steered back to its origin, recombine under the emission of a high-energy photon [1]. The process is coherent, so the result of the interaction is the production of high-frequency coherent radiation. The emitted signal can be used to create coherent UV or XUV pulses, and this radiation may then, e.g., in fundamental science, be utilized to probe ultrafast attosecond electron dynamics (see Refs. [2,3] for recent reviews).

As compared to atoms, diatomic molecules possess additional degrees of freedom, namely the nuclear separation and the orientation with respect to the laser field. Studies of HHG from the H_2^+ molecular ion [4–6] along with the molecules N_2 and O_2 [7,8] show that the extra parameters of the molecules give rise to additional effects on the harmonic spectrum. There are two reasons why this complex behavior for molecules is of interest: (i) the extra parameters available for manipulating HHG from the molecules may be useful tools for controlling the intensity of the harmonics; and (ii) the fact that the harmonic spectrum contains features reminiscent of the molecular structure means that the emitted signals provide a way to study the nuclear motion and attosecond electron dynamics of the source of the high-harmonic radiation [9–12].

The complete theoretical modeling of HHG is computationally very challenging. In *ab initio* approaches the time-dependent Schrödinger equation has to be propagated in a box much larger than is the case for strong-field ionization studies since in the former case one has to make sure that the electronic wave packet does not engage with an absorbing boundary. Additional complications come from the subsequent propagation of Maxwell's equations in the generating medium, and in any case going beyond an effective one-electron model, or other reduced dimensionality models, seems impossible in the foreseeable future. These complications underline the importance of developing accurate approximate theories. In particular for molecules, such models, which should be relatively inexpensive to evaluate, are of interest since investigations aiming, e.g., at an increased degree of control of the harmonic production, require a set of evaluations for different bond lengths and orientations with respect to the field. In this paper we present one such theory. We provide a model to calculate the angular dependence of the harmonic signal from a single diatomic molecule of arbitrary orientation with respect to the laser field. In particular we include the effect of nuclear motion (vibration), and we test the accuracy of the model by comparison with experiments. High-harmonic generation from diatomic molecules has already been considered in an extension of the Lewenstein model [13] in Ref. [7]. In that work depletion from the initial state was considered but the nuclear motion was ignored. Recently, the strong-field approximation (SFA) for HHG in diatomic molecules subject to ultrashort laser pulses was presented, again ignoring nuclear motion, but combined with a careful saddle-point analysis and a discussion of the gauge problem [14]. Here, we are concerned with the response to a monochromatic field, and in parallel with the conventions in the theory of strong-field ionization, we will refer to our theory as the length gauge version of the molecular SFA for HHG.

The present paper is organized as follows. In Sec. II we present the theory for HHG from diatomic molecules in monochromatic linearly polarized laser fields. Section III contains some calculational details. In Sec. IV we show the HHG yields for N_2 and O_2 as a function of the orientation of the molecules with respect to the laser polarization, and compare with experimental measurements. By discussing HHG signals from the isotopes H_2 and D_2, we also see how a difference in nuclear mass affects the harmonic spectrum. The paper ends with a summary and a conclusion in Sec. V. Appendix contains a discussion of the momentum space wave function of a molecule in the single-active-electron (SAE) approximation.

II. THEORY

In our treatment of the HHG from molecules, we extend the atomic model of Ref. [15], and include notions of nuclear motion. We consider the case where the laser pulse contains several cycles such that a Floquet approach is suitable. As we shall see below when we compare with experimental results,

even for probe pulses of 50 fs [11] and 35 fs [12] duration, this turns out to be an accurate approximation. Hence using the Coulomb gauge and the dipole approximation, a laser field with frequency ω and period $T=2\pi/\omega$ is described by the vector potential $\mathbf{A}(t)=\mathbf{A}_0\cos(\omega t)$. The electric field, $\mathbf{F}(t)$, is then $-\partial\mathbf{A}(t)/\partial t$, i.e., $\mathbf{F}(t)=\mathbf{F}_0\sin(\omega t)$ with $\mathbf{F}_0=\omega\mathbf{A}_0$ (atomic units, $e=\hbar=m_e=a_0=1$, are used throughout unless indicated otherwise).

The harmonic generation is determined by the dipole moment

$$d(t)=\langle\Psi(t)|\hat{D}_{\epsilon}^{(n)}|\Psi(t)\rangle, \tag{1}$$

where the dipole operator is defined by

$$\hat{D}_{\epsilon}^{(n)}=\sum_{i=1}^{n}\hat{d}_{\epsilon,i}=\sum_{i=1}^{n}\boldsymbol{\epsilon}\cdot\mathbf{r}_i, \tag{2}$$

with $\boldsymbol{\epsilon}$ the polarization vector of the field, and where $|\Psi(t)\rangle$ is the solution to the n-electron Schrödinger equation for the diatomic molecule

$$\left[i\frac{\partial}{\partial t}-H_0-V_F^{(n)}\right]\Psi(\mathbf{r}_1,\mathbf{r}_2,\ldots,\mathbf{r}_n,\mathbf{R},t)=0, \tag{3}$$

with $\mathbf{r}_i$ the coordinate of electron i, and $\mathbf{R}$ the relative position of the two nuclei, H_0 the field-free part of the Hamiltonian of the molecule, and $V_F^{(n)}$ the interaction of the molecule with the laser field. In the present length gauge description

$$V_F^{(n)}=\mathbf{F}(t)\sum_{i=1}^{n}\mathbf{r}_i. \tag{4}$$

From Eq. (1) it is clear that in order to obtain the dipole moment, we need a solution of Eq. (3). The state $|\Psi(t)\rangle$ is determined by using the description of the laser-molecule system given in Ref. [16]. Here nuclear motion is modeled within the Born-Oppenheimer (BO) approximation, and, assuming negligible electron-electron correlation, the electrons are put into orbitals obtained from Hartree-Fock (HF) calculations. Consequently, the interaction of the molecule can be treated in the SAE approximation, where the active electron is the electron in the highest occupied molecular orbital (HOMO). We write $|\Psi(t)\rangle$ as a superposition of the field-free state of the molecule and final states, where the active electron is excited to the continuum. The expansion coefficients are obtained under the assumption that there is only limited ionization, which again requires that the laser intensity is below saturation (the regime of relevance in the HHG process). Inserting the expanded state into Eq. (1), we arrive at the following approximation to the dipole moment:

$$d_0(t)=-i\int_{-\infty}^{t}dt'\sum_{\nu_i}\int d\mathbf{q}\langle\Phi_0(t)|\hat{D}_{\epsilon}^{(n)}|\Psi_{\nu_i\mathbf{q}}(t)\rangle \times\langle\Psi_{\nu_i\mathbf{q}}(t')|V_F^{(n)}(t')|\Phi_0(t')\rangle. \tag{5}$$

Here

$$\Phi_0=\frac{1}{\sqrt{n!}}\det[\phi_1(\mathbf{r}_1;R_0)\phi_2(\mathbf{r}_2;R_0)\cdots\phi_n(\mathbf{r}_n;R_0)] \times\chi_{\nu_0}(R)\exp(-iE_0t) \tag{6}$$

is the field-free ground state of total energy $E_0=E_0^e(R_0)+E_{\nu_0}$, where $E_0^e(R_0)$ denotes the electronic eigenenergy at nuclear equilibrium distance R_0, and E_{ν_0} is the vibrational eigenenergy of the nuclear Hamiltonian. The electronic part of this state is expressed as a Slater determinant of the orbitals $\phi_j(\mathbf{r}_i;R_0)$, while $\chi_{\nu_0}(R)$ denotes the vibrational ground state wave function, labeled by vibrational quantum number ν_0. Furthermore,

$$\Psi_{\nu_i,\mathbf{q}}=\frac{1}{\sqrt{n!}}\det[\phi_1(\mathbf{r}_1;R_0)\phi_2(\mathbf{r}_2;R_0)\cdots\Phi_{\mathbf{q}}(\mathbf{r}_n,t)] \times\chi_{\nu_i}^{+}(R)\exp(-iE^{+}t) \tag{7}$$

is the state of the molecule interacting with the laser field and $E^{+}=E^{e,+}(R_0)+E_{\nu_i}^{+}$ is the total energy of the residual molecular ion. We also introduced $\Phi_{\mathbf{q}}$, which denotes the state of the active electron, and we neglect the interaction of this electron with the residual molecular ion. Then the state of the active electron is given by a Volkov wave

$$\Phi_{\mathbf{q}}(\mathbf{r},t)=\frac{1}{(2\pi)^{3/2}}\exp\left\{i\left[[\mathbf{q}+\mathbf{A}(t)]\cdot\mathbf{r}-\mathbf{q}\cdot\boldsymbol{\alpha}_0\sin(\omega t)-\frac{U_p}{2\omega}\sin(2\omega t)-\left(\frac{q^2}{2}+U_p\right)t\right]\right\}, \tag{8}$$

with quiver radius $\boldsymbol{\alpha}_0=\mathbf{A}_0/\omega$ and ponderomotive potential $U_p=A_0^2/4$.

Using the Slater-Condon rules [17], the expression in Eq. (5) reduces to an expression involving only the electron coordinate of the active electron

$$d_0(t)=-i\sum_{\nu_i}\int_{-\infty}^{t}dt'\int d\mathbf{q}\langle\nu_0|\nu_i\rangle\langle\phi_0(\mathbf{r};R_0)|\hat{d}_{\epsilon}|\Phi_{\mathbf{q}}(\mathbf{r},t)\rangle \times\exp\{i[E_0^e(R_0)+E_{\nu_0}-E^{e,+}(R_0)-E_{\nu_i}^{+}]t\} \times\langle\nu_i|\nu_0\rangle\langle\Phi_{\mathbf{q}}(\mathbf{r}',t')|V_F(t')|\phi_0(\mathbf{r}';R_0)\rangle \times\exp\{-i[E_0^e(R_0)+E_{\nu_0}-E^{e,+}(R_0)-E_{\nu_i}^{+}]t'\}. \tag{9}$$

To simplify notation, we have dropped the index of the electron and consequently introduced $\hat{d}_{\epsilon}=\boldsymbol{\epsilon}\cdot\mathbf{r}$, $V_F(t')=\mathbf{F}(t')\cdot\mathbf{r}'$. Also we denote the HOMO wave function by $\phi_0(\mathbf{r})$, and

$$\langle\nu_i|\nu_0\rangle=\int_0^{\infty}dR\chi_{\nu_i}^{+*}(R)\chi_{\nu_0}(R) \tag{10}$$

denotes the Franck-Condon (FC) factor.

A. The harmonics and the three-step picture

The harmonic spectrum is calculated from the Fourier transform of the dipole moment $d_0(t)$, which implies that the intensity of the Nth harmonic is proportional to the norm square of the Nth Fourier component, d_N. This Fourier

component is investigated by extending the technique of Ref. [15] to the molecular case

$$d_N = \frac{1}{T}\int_0^T dt \exp(iN\omega t) d_0(t)$$
$$= -\sum_k \sum_{\nu_i} \frac{1}{T}\int_0^T dt \frac{1}{T}\int_0^T dt' \times (2\pi)^2 \langle \nu_0|\nu_i\rangle$$
$$\times \langle \phi_0(\mathbf{r})|\exp(iN\omega t)\hat{d}_\epsilon|\Phi_{\mathbf{K}_k^{\nu_i}}(\mathbf{r},t)\rangle \exp\{i[E_0^e(R_0)$$
$$+ E_{\nu_0} - E^{e,+}(R_0) - E_{\nu_i}^+]t\}\frac{1}{L_0(t,t')}\langle \nu_i|\nu_0\rangle$$
$$\times \langle \Phi_{\mathbf{K}_k^{\nu_i}}(\mathbf{r}',t')|V_F(t')|\phi_0(\mathbf{r}')\rangle \exp\{i[E^{e,+}(R_0)$$
$$+ E_{\nu_i}^+ - E_0^e(R_0) - E_{\nu_0}]t'\}. \quad (11)$$

An interpretation of Eq. (11) is possible in terms of the three-step picture of HHG. The matrix element $\langle \Phi_{\mathbf{K}_k^{\nu_i}}(\mathbf{r}',t')|V_F(t')|\phi_0(\mathbf{r}')\rangle$ describes the transition from the HOMO and into the field-dressed Volkov state with momentum of magnitude

$$K_k^{\nu_i} = \sqrt{2[k\omega + E_0^e(R_0) + E_{\nu_0} - E^{e,+}(R_0) - E_{\nu_i}^+ - U_p]}. \quad (12)$$

The direction of the momentum is parallel or antiparallel (prescribed by the positive or negative sign of σ defined below) to the polarization vector of the laser field. This momentum emerges after performing the $\mathbf{q}$ integration in Eq. (9), provided that the laser field is sufficiently strong in the sense that the quiver radius, $\boldsymbol{\alpha}_0$, is large compared to the extent of the molecule. Following [15], we include only terms corresponding to real values of $K_k^{\nu_i}$, because of the clear physical interpretation of Eq. (11). The exponential of the last line of Eq. (11) describes the energy balance in this initial step, and $\langle \nu_i|\,\nu_0\rangle$ is the FC factor associated with the transition in the nuclear degree of freedom. The factor $1/L_0(t,t')$ with $L_0(t,t')=\sigma\alpha_0(\sin\omega t' - \sin\omega t)$ and $\sigma=\pm 1$ to assure $\mathrm{Re}(L_0)>0$ comes from the Volkov propagator and describes the decrease of the amplitude of the continuum wave as the latter expands into three-dimensional space. Finally, the matrix element $\langle \phi_0(\mathbf{r})|\hat{d}_\epsilon|\Phi_{\mathbf{K}_k^{\nu_i}}(\mathbf{r},t)\rangle$ with associated phase factors and FC factor describes the laser-assisted recombination (LAR) step of the three-step model. We note that, in our model, the expression of Eq. (11) predicts a correlation of the momentum of the continuum electron with the nuclear motion of the residual molecular ion, through the oscillating time-dependent exponential factors.

B. The harmonic spectrum from arbitrarily oriented molecules

In order to be able to evaluate Eq. (11) for molecules of arbitrary orientation with respect to the laser field we use a HOMO wave function, where the angular part is expanded onto spherical harmonics. In the body-fixed frame, where the z axis is chosen along the internuclear axis, the HOMO wave function is then given by

$$\phi_0^{bf}(\mathbf{r}) = \sum_l F_{l,m}(r) Y_l^m(\hat{\mathbf{r}}). \quad (13)$$

We also need the asymptotic form of this expression

$$\phi_0^{bf}(\mathbf{r}) \sim \sum_l C_{l,m} r^{Z/\kappa - 1} \exp(-\kappa r) Y_l^m(\hat{\mathbf{r}}). \quad (14)$$

Here $\kappa=\sqrt{-2E_b}$, E_b is the binding energy of the active electron in the HF ground state wave function, and Z is the net charge of the molecule, when the HOMO electron is removed. The t' integral of Eq. (11) corresponds to the ATI step. It is well-known that in this process the HOMO electron escapes to the laser-dressed continuum, when the distance to the nucleus is large [18]. As a result we can employ the asymptotic form of the HOMO in the t' integrand in Eq. (11), and the integral will subsequently be evaluated using the saddle-point method. This evaluation proceeds as in Ref. [19], and the HOMO as given by Eq. (14) is replaced in favor of the momentum space wave function. It is sufficient to know the latter near its singular points, where it is given by the particularly simple expression Eq. (A4), as described in the Appendix. The t integration occurring in Eq. (11) corresponds to the LAR step and is performed numerically. Previous publications show that in the LAR step it is inadequate to approximate the HOMO with the asymptotic form, because the recombination takes place at small separations of the excited electron and the molecular core [6,20]. Also here we prefer to replace the space wave function from Eq. (13) by the momentum space wave function, which in the body fixed frame may be written in the following way:

$$\tilde{\phi}_0^{bf}(\mathbf{q}) = \sum_l G_{l,m}(q) Y_l^m(\hat{\mathbf{q}}), \quad (15)$$

where the $G_{l,m}$'s are obtained numerically. Because the HOMO wave functions are expressed in terms of spherical harmonics, we can easily obtain the wave functions of the molecule in the laboratory frame, where the internuclear axis does not necessarily coincide with the z axis. For a molecule, where the internuclear axis is rotated with respect to the z axis of the laboratory frame, the rotation is characterized by the three Euler angles $\mathcal{R}=(\alpha,\beta,\gamma)$ [21], and we arrive at the following expression of the Nth harmonic for a molecule of orientation $\mathcal{R}$ with respect to the laser polarization

$$d_N = \sum_{l_2,l_1}\sum_{m_2',m_1'} D^{l_2*}_{m_2',m_2}(\mathcal{R}) D^{l_1}_{m_1',m_1}(\mathcal{R}) C_{l_1,m_1} \sum_{\nu_i} |\langle \nu_i|\nu_0\rangle|^2$$
$$\times \sum_k \sum_{C(k)} \mathcal{B}^{N,\nu_i,k}_{l_2,m_2',m_2}[C(k)] \mathcal{A}^{\nu_i,k}_{l_1,m_1'}[C(k)], \quad (16)$$

with

TABLE I. The molecular properties used in this work for evaluation of HHG. I_p is the experimental adiabatic ionization potential, R_0 is the equilibrium distance, and B is the rotational constant of the molecule [24]. The parallel and perpendicular polarizabilities $\alpha_\parallel$ and $\alpha_\perp$ of N_2 and O_2 are based on values from [25] and [24], respectively. We furthermore give the angular coefficients $C_{l,m}$ from HF calculations. FC factors and vibrational energies can be found in the references indicated after each molecular species.

		I_p (eV)	R_0 (Å)	B (GHz)	$\alpha_\parallel$ (Å^3)	$\alpha_\perp$ (Å^3)	C_{00}	C_{2m}	C_{4m}
N_2 (σ_g)	[26]	15.58	1.098	59.647	2.38	1.45	3.46	1.64	0.12
O_2 (π_g)	[27]	12.03	1.208	42.861	2.3	1.1		1.04	0.07
H_2 (σ_g)	[28][a]	15.43	0.741				2.44	0.14	
D_2 (σ_2)	[28]	15.47	0.742				2.44	0.14	

[a]Vibrational energies from Ref. [29] are used.

$$\mathcal{A}^{\nu_i,k}_{l_1,m_1'}[C(k)] = -\frac{1}{T}\Gamma\left(1+\frac{Z/\kappa}{2}\right)2^{Z/\kappa/2}\kappa^{Z/\kappa}(\pm 1)^{l_1} \times \frac{\exp[iS(t'_{C(k)})]}{\sqrt{[-iS''(t'_{C(k)})]^{1+Z/\kappa}}} \times Y^{m_1'}_{l_1}(\hat{\mathbf{q}}')|_{\mathbf{q}'=\mathbf{K}^{\nu_i}_k+\mathbf{A}(t'_{C(k)})}, \quad (17)$$

and

$$\mathcal{B}^{N,\nu_i,k}_{l_2,m_2',m_2}[C(k)] = i\frac{(2\pi)^2}{T}\int_0^T dt \frac{\exp\{i[N\omega t - S(t)]\}}{L_0(t,t'_{C(k)})}(\boldsymbol{\epsilon}\cdot\nabla_{\mathbf{q}}) \times [G_{l_2,m_2}(q)Y^{m_2'}_{l_2}(\hat{\mathbf{q}})]^*|_{\mathbf{q}=\mathbf{K}^{\nu_i}_k+\mathbf{A}(t)}. \quad (18)$$

Here $D^{l}_{m_i',m_i}(\mathcal{R})$, $i=1,2$, denotes the matrix elements of the rotation operator [21] and

$$S(t) = k\omega t + \mathbf{K}^{\nu_i}_k\cdot\boldsymbol{\alpha}_0\sin(\omega t) + \frac{U_p}{2\omega}\sin(2\omega t) \quad (19)$$

is the quasiclassical action. The index $C(k)$ denotes the saddle-points. For each k the saddle-points $t'_C(k)$ are defined by the condition $S'[t'_C(k)]=0$, and we use the ones with $0\leqslant \mathrm{Re}[t'_C(k)]<T$ along with $\mathrm{Im}[t'_C(k)]>0$. Note that Eq. (17) is evaluated in the complex t' plane and the factor $(\pm 1)^{l_1}$ in Eq. (17) corresponds to the limits $\pm i\kappa$ of the size q' of the electron momentum at the saddle-points. Letting the laser polarization define the z axis of the laboratory frame, we have both the momentum of the Volkov wave as well as the vector potential parallel to the z axis, so that $Y^{m_1'}_{l_1}(\hat{\mathbf{q}}')\propto\delta_{m_1',0}$ in Eq. (17). Equation (18) is evaluated along the real t axis, and when the polarization vector of the field is directed along the z axis $\boldsymbol{\epsilon}\cdot\nabla_{\mathbf{q}}$ reduces to a partial derivative with respect to the size q of the momentum. As mentioned earlier we consider only values of k, where $K^{\nu_i}_k$ is real, which serves to define a lower limit k_{min} of the sum. The upper limit k_{max} is determined by requiring convergence of the calculated value of d_N. Equation (16) along with the accompanying definitions of Eqs. (17)–(19) summarize the formulation of our model. A cruder estimate of the harmonic generation can be obtained by using the asymptotic form of the HOMO wave function in both the ATI and the LAR step. In this approximation the Nth harmonic is given by

$$d^{as}_N = \sum_{l_2,l_1}\sum_{m_2',m_1'} D^{l_2*}_{m_2',m_2}(\mathcal{R})D^{l_1}_{m_1',m_1}(\mathcal{R})C^*_{l_2,m_2} \times C_{l_1,m_1}\sum_{\nu_i}|\langle\nu_i|\nu_0\rangle|^2\sum_k\sum_{C(k)}\tilde{\mathcal{B}}^{N,\nu_i,k}_{l_2,m_2'}[C(k)] \times \mathcal{A}^{\nu_i,k}_{l_1,m_1'}[C(k)], \quad (20)$$

with

$$\mathcal{B}^{N,\nu_i,k}_{l_2,m_2'}[C(k)] = -\frac{\sqrt{2}(2\pi)^2}{T}\int_0^T dt\frac{\exp\{i[N\omega t - S(t)]\}}{L_0[t,t'_C(k)]}(-i\boldsymbol{\epsilon}\cdot\nabla_{\mathbf{q}}) \times \left[\left(\frac{q}{i\kappa}\right)^{l_2}\frac{1}{2^{l_2+1}\kappa^{2+Z/\kappa}}\frac{\Gamma(l_2+2+Z/\kappa)}{\Gamma\left(l_2+\frac{3}{2}\right)}Y^{m_2'}_{l_2}(\hat{\mathbf{q}}) \times {}_2F_1\left(\frac{l_2+2+Z/\kappa}{2},\frac{l_2+2+Z/\kappa}{2}+\frac{1}{2};l_2+\frac{3}{2};-\left(\frac{q}{\kappa}\right)^2\right)\right]^*\Bigg|_{\mathbf{q}=\mathbf{K}^{\nu_i}_k+\mathbf{A}(t)}, \quad (21)$$

where all functions are analytically known and where the C_{lm} parameters are available in Table I (see also Table I in Ref. [16]). The asymptotic expression in Eq. (20) has the advantage that all geometric factors are pulled outside the integration.

In Sec. IV we compare HHG spectra obtained with the two forms of Eqs. (16) and (20). In that section we also show curves, which do not include nuclear motion. When the nuclei are clamped, the harmonic strengths are simply given by including only the first term in the sum over ν_i in Eqs. (16) and (20) and replacing the Franck-Condon factors by unity.

III. CALCULATIONAL DETAILS

In this section we outline some calculational details to be used below. First we sketch the procedure used to obtain the $G_{l,m}(q)$'s and $C_{l,m}$'s of Eqs. (16) and (20). The initial step in the procedure is to solve the HF equations fully numerically for the diatomic molecules [22]. In this manner the ground state orbitals are obtained, and are projected onto spherical harmonics to attain the radial functions $F_{l,m}(r)$. The

asymptotic angular coefficients are found by comparing the HF radial wave functions with the form $C_{l,m}r^{Z/\kappa-1}\exp(-\kappa r)$, where the $C_{l,m}$'s are used as fitting parameters. The $G_{l,m}(q)$'s, on the other hand, are obtained from the Fourier-Bessel transform of the $F_{l,m}(r)$'s.

In the cases of N_2 and O_2 we compare results of our model with experiments where the degree of molecular alignment was controlled by nonadiabatically creating a rotational wave packet by a pump pulse and then monitoring the harmonic yield as a function of the time delay to the intense probe pulse [11,12]. In order to perform a comparison with the experimental results, we need the time-dependent angular distribution $\rho(t,\beta)$ of the rotational wave packet created by the pump pulse. We refer to Ref. [23] for details about calculations of rotational wave packets. We assume that rotation is negligible under the probe pulse, and simply note at this point that once the angular distribution is available, the amplitude of the Nth harmonic at time t is given by

$$\bar{d}_N(t) = \int_0^\pi d\beta \sin(\beta)\rho(t,\beta)d_N(\beta), \tag{22}$$

where $d_N(\beta)$ can be found using Eq. (16) for a probe laser parallel to the pump laser. We can then calculate the intensity of each harmonic from the rotational wave packet at every point of time.

Table I shows relevant information for the calculations presented in the next section.

IV. RESULTS AND DISCUSSION

A. The N_2 molecule

We begin by presenting a calculation of HHG from the N_2 molecule with a HOMO of σ_g symmetry. The laser is assumed to have an energy of $\omega=0.057$ a.u. corresponding to a wavelength of $\lambda=800$ nm, and the intensity is taken to be $I=2\times10^{14}$ W/cm^2 which is well below the saturation laser intensity [12]. Such a choice of parameters is within the range of a Ti:sapphire laser. Figure 1 shows the relative strength of the harmonics as a function of the harmonic order in a geometry, where the internuclear axis of the molecule is aligned parallel to the polarization of the laser ($\beta=0°$). Note that we refer to the norm square of the Fourier components (i.e., $|d_N|^2$) as the strength of the harmonics. There are three different curves on the figure, and the dotted curve corresponds to Eq. (20), i.e., the case where the asymptotic wave function is used in both the ATI and LAR step of the HHG process, while the dashed and solid curves correspond to Eq. (16) meaning that the improved wave function was employed in the LAR step. Calculations represented by the solid curve take nuclear motion into account. The harmonic spectrum of the N_2 molecule is different, when the asymptotic wave function is used everywhere as compared to the case, when the improved wave function is employed in the LAR step. This result shows that the quality of the HOMO wave function is of importance. It is also clear from Fig. 1 that the effect of nuclear motion in the case of N_2 is negligible. This is because the BO potential energy curves of

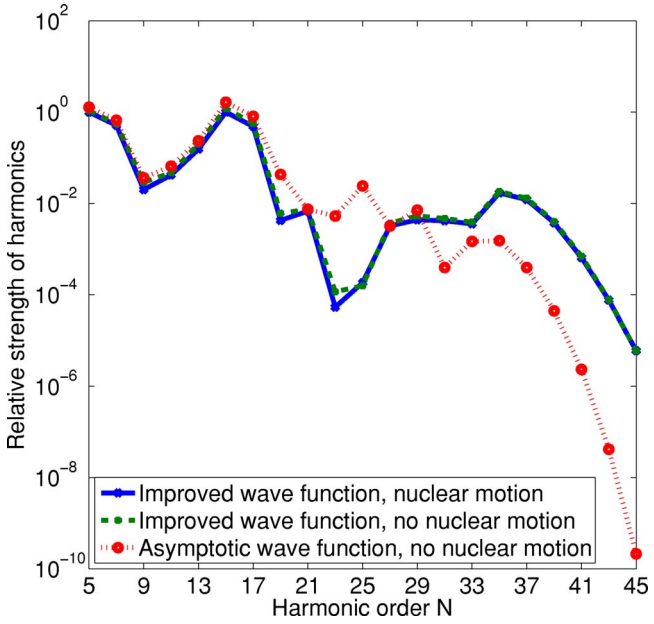

FIG. 1. (Color online) Comparison of HHG from the N_2 molecule when using the asymptotic wave function in both the LAR and ATI step, and when the wave function used in the LAR step is improved. Only the solid curve includes nuclear motion. The signals have been normalized to the strength of the fifth harmonic obtained by using the improved wave function in the LAR step and including nuclear motion. The internuclear axis and the polarization are parallel ($\beta=0°$).

the N_2 molecule and the N_2^+ molecular ion are nearly parallel, which means that ionization of an N_2 molecule in the ground state always leaves the residual molecular N_2^+ ion in the vibrational ground state.

In Fig. 2 we study the orientation dependence of the HHG yield from N_2. It is seen from the figure that harmonic generation for the parallel alignment ($\beta=0°$) is more intense than the harmonic generation for the perpendicular alignment ($\beta=90°$), which reflects the orientation dependence of the ionization of the molecule (see Ref. [30] and references therein). The detailed angular behavior depends on the harmonic order in consideration: a minimum is observed at approximately 40° for some orders. A similar behavior was recently predicted in Ref. [7], where the minima were located at a relative orientation close to 60°.

Several experiments have measured the harmonic emission from nonadiabatically aligned N_2 molecules [11,12,31]. We can simulate these results as outlined in Sec. III. To compare with the results of Ref. [12] we use the time-dependent angular distribution $\rho(t,\beta)$ corresponding to a rotational wave packet created by the experimental pump pulse, 60 fs, 800 nm, intensity 4×10^{13} W/cm^2, and the experimental initial rotational temperature of N_2 of 30 K. To model the results from Ref. [11] we obtain the time-dependent angular distribution with the experimental pump pulse of duration 50 fs and with wavelength 800 nm and intensity 6×10^{13} W/cm^2. In Eq. (22) the value of $d_N(\beta)$ is calculated using Eq. (16) for a laser of wavelength $\lambda=800$ nm and intensity $I=2\times10^{14}$ W/cm^2, as in Refs. [11,12]. We can then find the intensity of each harmonic from the rotational wave

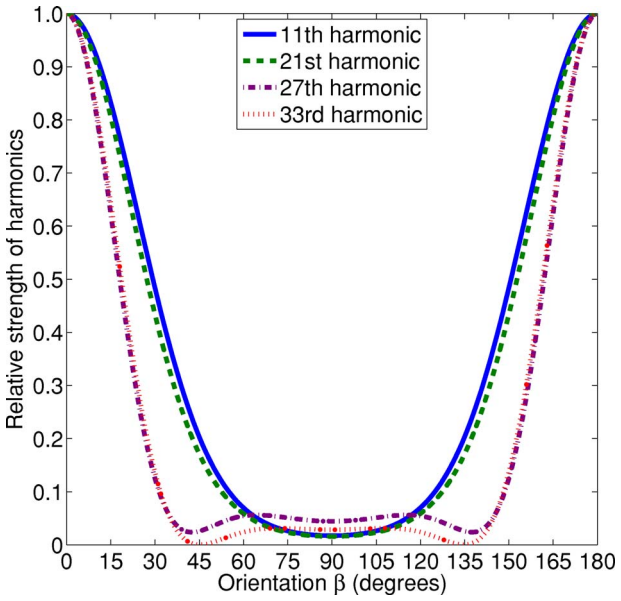

FIG. 2. (Color online) Orientation dependence of the harmonics for the molecule N_2. We have employed the improved wave function in the LAR step and included nuclear motion. All curves are normalized to their respective values at $\beta=0°$.

packet at every point of time. In Fig. 3 we compare model calculations with experimental results. The figure shows the evolution of the harmonic emission from the N_2 molecule as a function of the delay time between the pump and probe pulse. In general the agreement between experiments and theory is very satisfactory.

B. The O_2 molecule

We next consider the O_2 molecule, which has a HOMO with π_g symmetry. The laser parameters are the same as in the preceding section. Figure 4 shows the relative strength of the harmonics for $\beta=36°$. As in the case of N_2 it is important to use a better wave function than the asymptotic one in the LAR step. The effect of nuclear motion is more pronounced than for the N_2 molecule because the Franck-Condon distribution of O_2 is broader than that of the N_2 molecule (see Ref. [32] for more discussion on the implications on final state vibrational levels and possible control of these).

We now turn to the angular dependence of the harmonics. The strength of some selected harmonics as a function of the orientation with respect to the laser field is shown in Fig. 5. It is possible to understand the results of Fig. 5 from the symmetry of the HOMO. The π_g symmetry means that the HOMO has nodes along the internuclear axis as well as perpendicular to it, and this leads to a vanishing harmonic generation when $\beta=0°$ and 90°. Consequently the harmonics take on maximal values for intermediate angels. All harmonics are most intense at orientations near 45°. It is also worth noticing that the precise location of the individual peak depends slightly on the order of the harmonic. This reflects that higher harmonics probe regions closer to the core.

For the O_2 molecule, as well, several measurements of HHG from a nonadiabatically aligned sample have been carried out [11,12,31]. We compare our model calculations with the results presented in Ref. [11] in the case of HHG from O_2. In retrieving the time-dependent angular distribution we use the experimental pump pulse of 50 fs with wavelength 800 nm and intensity 6×10^{13} W/cm^2. We calculate the value of $d_N(\beta)$ for use in Eq. (22) under assumptions corresponding to the experimental probe pulse with wavelength $\lambda=800$ nm and intensity $I=2\times10^{14}$ W/cm^2. As in the case of N_2 above, we normalize the harmonic intensity to the intensity of a randomly aligned sample in our theoretical results. The comparison is shown in Fig. 6, and we observe a fine agreement between theory and experiment.

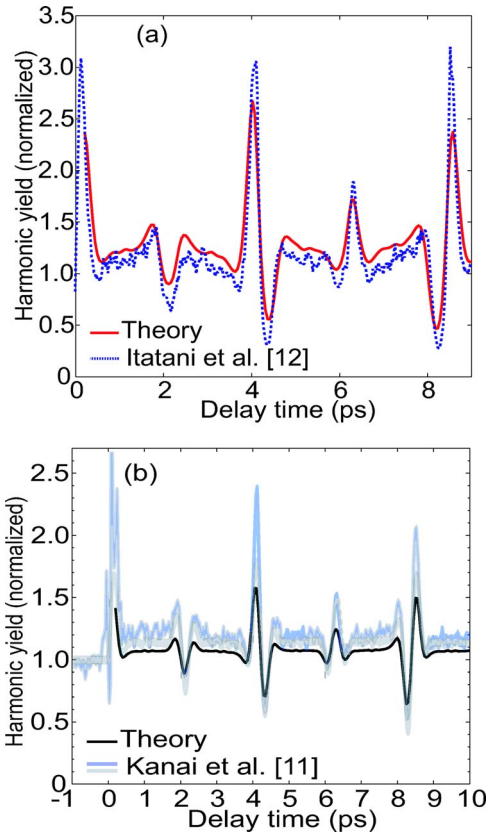

FIG. 3. (Color online) Comparison of theory and experiment in the case of N_2. Panel (a) shows the average of the 21st to the 25th harmonics from a rotational wave packet of N_2. Theoretical results are based on our model, while the results of Itatani *et al.* are experimental data from Ref. [12]. In panel (b) the 23rd harmonic according to our model is compared with the experimental results of Ref. [11]. Our results are normalized to the randomly aligned case.

C. The isotopic molecules H_2 and D_2

We now turn to a short discussion of calculations carried out for HHG from the isotopic molecules H_2 and D_2. Harmonic spectra from these molecules provide a way to study the effect of nuclear motion, because the FC distributions of both H_2 and D_2 are broad. Furthermore, a comparison of the HHG signals from the isotopes contains information on how the nuclear masses affect the harmonic spectrum.

In Fig. 7, showing HHG from the H_2 molecule, we have used the same laser parameters as in the case of N_2 and O_2

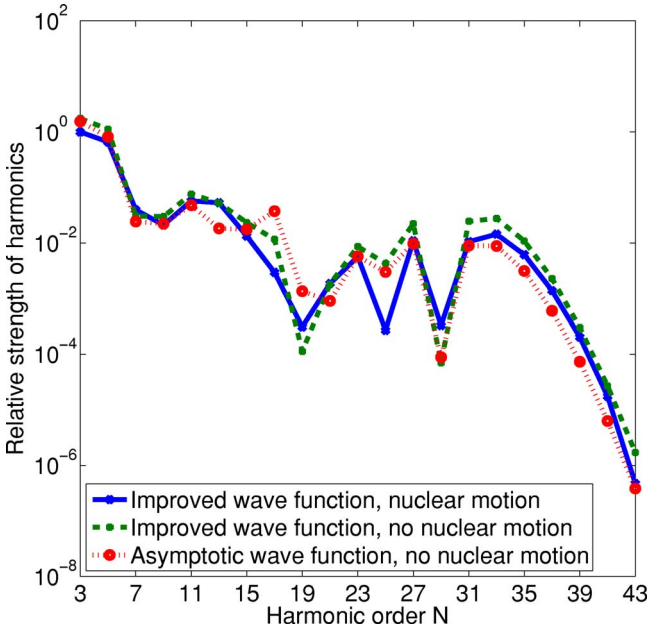

FIG. 4. (Color online) HHG from the O_2 molecule. The strength of the harmonics is normalized to the strength of the third harmonic obtained in the calculation, where an improved wave function is used in the LAR step and the nuclear motion is included. The internuclear axis is oriented at an angle $\beta=36°$ with respect to the internuclear axis. See text for further details.

studied above, i.e., 800 nm, 2×10^{14} W/cm^2. As seen from the figure, it is essential to include nuclear motion in the case of H_2, and the general effect of the nuclear motion is to reduce the intensity of harmonic generation. This can easily be understood from the fact that the FC distributions of the isotope are broad. The broadness implies that a substantial

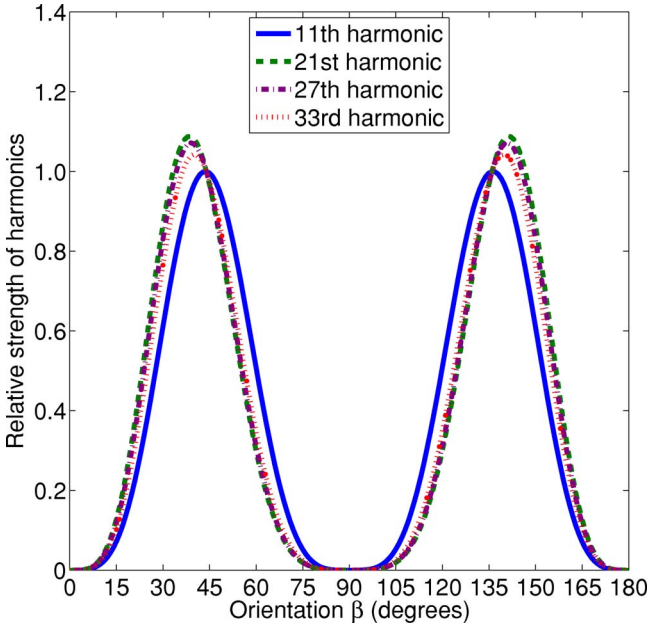

FIG. 5. (Color online) HHG from the O_2 molecule as a function of the orientation. The strength of the harmonics are calculated using Eq. (16). All curves are normalized to their value at $\beta=45°$.

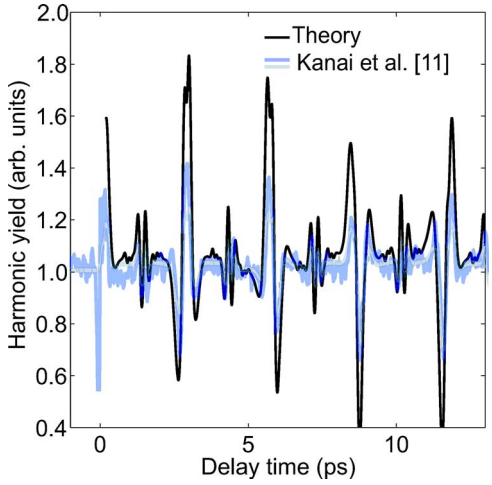

FIG. 6. (Color online) Comparison of our model calculations with the experimental results from Ref. [11] in the case of O_2. We have calculated the intensity of the 23rd harmonic from a rotational wave packet of O_2 normalized against the randomly aligned case.

part of the harmonic signal originates from transitions, where the ionization potential is higher than in the fixed nuclei picture. As a result the whole process gets more unlikely and so the radiative emission is less intense. Very similar observations and conclusions hold true in the case of D_2.

To see how the nuclear mass influences HHG, we compare the harmonic generation of the two isotopes for different intensities at a laser energy of $\omega=0.057$ a.u. in a geometry, where the internuclear axes of the molecules are aligned perpendicular to the laser polarization. In order to be able to compare with results of Ref. [8] we have furthermore in-

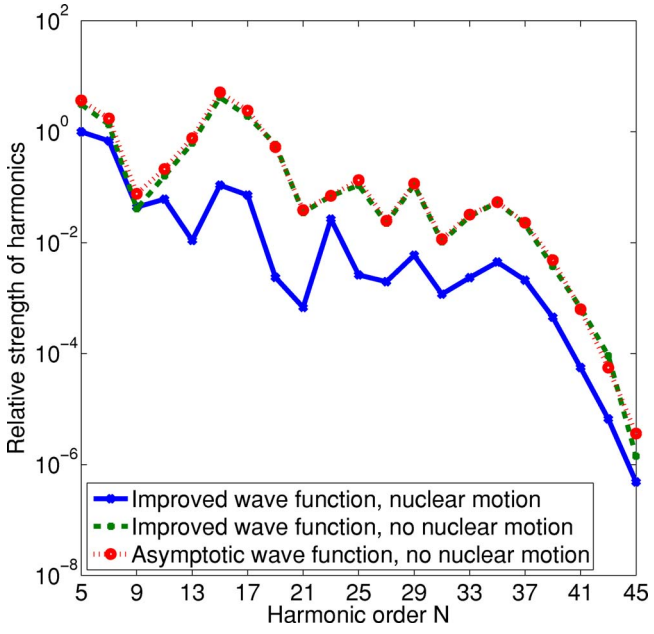

FIG. 7. (Color online) HHG from the H_2 molecule. Calculations are performed under the setup mentioned in the text, and all curves are normalized to the strength of the fifth harmonic obtained by using the improved wave function in the LAR step and taking into account the effect of nuclear motion.

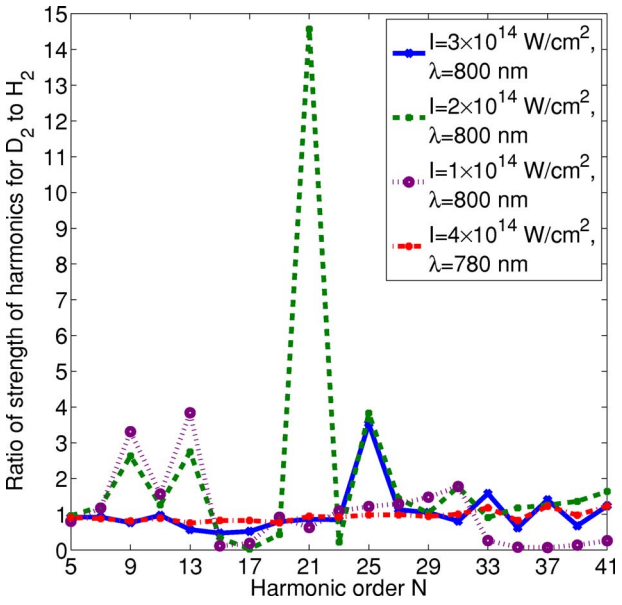

FIG. 8. (Color online) Comparison of harmonic generation for the isotopes H_2 and D_2 for different intensities at orientation $\beta=90°$. The ordinate shows the strength of the Nth harmonic of D_2 divided by the strength of the Nth harmonic of H_2. The laser parameters for the dash-dotted curve are the same as those used in Ref. [8].

cluded a calculation at intensity $I=4\times10^{14}$ W/cm^2 at energy $\omega=0.0584$ a.u., although our assumption of negligible depletion of the ground states is questionable in this situation. The results are shown in Fig. 8. In Ref. [8] a two-dimensional model was used and it was found that the heavier isotope leads to stronger harmonic generation. We cannot conclude something as simple from Fig. 8. Our nonconclusive picture of the relation between nuclear mass and HHG is supported by others [33], and is related to the strong correlation of the vibrational states of the residual molecular ion to the momentum of the excited electron as follows from Eq. (11).

V. SUMMARY AND CONCLUSION

We have developed the strong-field approximation for HHG in diatomic molecules for calculating the harmonic signal from a single diatomic molecule of arbitrary orientation with respect to a monochromatic linearly polarized laser field. The model incorporates the effect of nuclear motion.

We calculated the high-harmonic emission from the molecules N_2, O_2, H_2, and D_2. The two latter species were considered in order to study the effect of nuclear motion in detail. The effect of nuclear motion on these light molecules was significant and generally reduced the intensity of the harmonics. However, there seems to be no simple common relation between nuclear mass and the intensity of the harmonic generation.

Turning to the N_2, O_2 cases, we successfully employed the present model to reproduce experimental results on HHG from nonadiabatically aligned N_2 and O_2 molecules [11,12]. The spectra for N_2 were very sensitive to the quality of the wave functions used to describe the molecule, while the effect of nuclear motion was small. The intensity of the harmonics was generally weaker, when the angle between the laser polarization and the internuclear axis was 90° as compared to the intensity at an angle of 0°. This orientation dependence characterizes diatomic molecules with a HOMO of σ_g symmetry. We also studied the orientation dependence of the harmonics for the O_2 molecule, where the HOMO has π_g symmetry. As in the case of N_2, the quality of the wave functions, used to model the O_2 molecule, was of importance, but furthermore we observed some effect of the nuclear motion on the harmonic emission. The π_g symmetry of the O_2 molecule revealed itself through the angular dependence of the harmonics. In the case of O_2 the harmonic generation was suppressed at orientations corresponding to both perpendicular as well as parallel alignment of the internuclear axis to the laser polarization. In support to earlier work [7], our results show that it is mainly the symmetry of the HOMO that determines the alignment dependence of the HHG.

To conclude, we have presented a length gauge strong-field approximation for HHG in diatomic molecules. The theory is very versatile and readily adapted to a wide range of diatomic molecules, and straightforwardly generalized to polyatomic molecules. The agreement with recent pump-probe experiments [11,12] is excellent, and hence we have confidence in the predictive power of the model. Despite the good agreement, it is clear that the model poses important questions, in particular concerning the fact that our model is formulated in the length gauge. This seems to be advantageous for the initial ionization step in order to obtain the correct orientation dependence in the process, and it is also physically well-justified since the ionization is tunneling like and the escape into the continuum happens at large distances, where the length gauge interaction has large weight [16]. The physics in the recombination step, however, is in a sense completely the opposite. In this case an effective transfer of momentum has to take place between the recombining electron and the core. Such a process is expected to be better described in the velocity gauge which naturally probes regions in space where the electron experiences abrupt changes (close to the nuclei).

Another point is the question of how to treat the nuclei. The present formalism gives an attempt in that direction: within the Born-Oppenheimer approximation, we applied the Franck-Condon principle and observed significant effects of the nuclear motion only for the lighter species H_2, and D_2. If it holds true then nuclear motion is essentially unimportant for all heavier systems, and it means that we may think of the nuclei as stationary fixed-in-space objects setting up an effective diffractionlike grating for the backscattered electron. Of course the outcome of the rescattering be it HHG or, e.g., future ionization, will be highly sensitive to this spatial arrangement, and this will undoubtedly lead to a higher degree of control of the harmonics.

ACKNOWLEDGMENTS

We would like to thank T. K. Kjeldsen and C. Z. Bisgaard for their contributions to the results presented in Sec. IV.

L.B.M. is supported by the Danish Natural Science Research Council (Grant No. 21-03-0163) and the Danish Research Agency (Grant. No. 2117-05-0081).

APPENDIX: THE ASYMPTOTIC MOLECULAR WAVE FUNCTION

In this appendix we work out the asymptotic form of the momentum space wave function of the HOMO and describe how this expression reduces to a well-known function around singular points [19]. We start out in the body fixed frame of the molecule with the z axis chosen along the internuclear axis. The HOMO wave function in position representation must then follow the asymptotic Coulomb form

$$\phi_0^{bf}(\mathbf{r}) \sim \sum_l C_{l,m} r^{Z/\kappa-1} \exp(-\kappa r) Y_l^m(\hat{\mathbf{r}}), \tag{A1}$$

where $\hat{\mathbf{r}}$ is a unit vector in direction of $\mathbf{r}$, $-\kappa^2/2=E_b$ is the binding energy of the HOMO-electron, and Z is the net charge of the molecule, when the HOMO electron has been removed. $Y_l^m(\hat{\mathbf{r}})$ is a spherical harmonic. The summation is over the set of l's such that $C_{l,m}\neq 0$. In this paper we are concerned with terms corresponding to $l=0,2,4$ (cf. Table I).

The Fourier transform of Eq. (A1) yields the momentum space wave function

$$\tilde{\phi}_0^{bf}(\mathbf{q}) \sim \sum_l \sqrt{2} C_{lm} \left(\frac{q}{i\kappa}\right)^l \frac{1}{2^{l+1}\kappa^{2+Z/\kappa}} \frac{\Gamma(l+2+Z/\kappa)}{\Gamma\left(l+\frac{3}{2}\right)} Y_l^m(\hat{\mathbf{q}}) \times {}_2F_1\left(\frac{l+2+Z/\kappa}{2}, \frac{l+2+Z/\kappa}{2}+\frac{1}{2}; l+\frac{3}{2}; -\left(\frac{q}{\kappa}\right)^2\right), \tag{A2}$$

where $\hat{\mathbf{q}}$ is a unit vector in the direction of $\mathbf{q}$. By evaluating Gauss' hypergeometric functions of type ${}_2F_1(a,a+1/2;l+3/2;z^2)$ and then inserting $a=(l+2+Z/\kappa)/2$ and $z^2=-(q/\kappa)^2$ we can obtain an explicit representation of the Fourier transform in Eq. (A2). To determine an expression of Gauss' hypergeometric function we have used formulas (15.1.9) and (15.1.10) in Ref. [34] along with a recursion relation coming from formula (9.137,1) in Ref. [35]. Consequently, we obtained expressions of type

$$\begin{aligned} &{}_2F_1\left(a, a+\frac{1}{2}; \frac{2n+1}{2}; z^2\right) \\ &= (-1)^n \frac{(2n-1)(2n-3)\cdots 3}{2} (1-z^2)^{n-2a} z^{-n} \\ &\times [2a-(2n-1)]^{-1}[2a-(2n-2)]^{-1} \\ &\times [2a-(2n-3)]^{-1}\cdots(2a-1)^{-1} \\ &\times \left[\frac{\mathcal{P}[+,2(n-1)]}{[z(1+z)]^{n-1}}(1-z)^{2a-n} - \frac{\mathcal{P}[-,2(n-1)]}{[z(1-z)]^{n-1}}(1+z)^{2a-n}\right], \end{aligned} \tag{A3}$$

where $\mathcal{P}[\pm,2(n-1)]$ is a polynomial of degree $2(n-1)$. The first five of these polynomials are given in Table II.

TABLE II. Polynomials of Eq. (A3) for use in the asymptotic form of the HOMO momentum space wave functions.

n	$\mathcal{P}[\pm,2(n-1)]$
1	1
2	$1\pm(2a-1)z+(2a-2)z^2$
3	$3\pm 3(2a-1)z+(4a^2-7)z^2\pm(8a^2-18a+7)z^3+(4a^2-12a+8)z^4$
4	$15\pm 15(2a-1)z+6(4a^2-a-8)z^2\pm 2(4a^3+12a^2-55a+24)z^3+(24a^3-72a^2+6a+57)z^4$ $\pm(24a^3-120a^2+168a-57)z^5+8(a^3-6a^2+11a-6)z^6$
5	$105\pm(210a-105)z+15(12a^2-4a-29)z^2\pm 5(16a^3+24a^2-190a+87)z^3+(16a^4+160a^3-760a^2+200a+699)z^4$ $\pm(64a^4-160a^3-640a^2+1750a-699)z^5+(96a^4-640a^3+1140a^2-140a-561)z^6$ $\pm(64a^4-560a^3+1640a^2-1810a+561)z^7+16(a^4-10a^3+35a^2-50a+24)z^8$

We are also interested in the limit $q\to\pm i\kappa$ corresponding to singularities of the asymptotic wave function because this expression is used for the HOMO wave function in Sec. II when the t' integration is evaluated by the saddle-point method. The continuation of Eq. (A2) to the complex $\mathbf{q}$ plane is straightforward [36]. Around the points of singularity Eq. (A2) can be written as [19]

$$\tilde{\phi}_0^{bf}(\mathbf{q}) \sim \sum_l \left(\frac{2}{\pi}\right)^{1/2} C_{l,m}(\pm 1)^l Y_l^m(\hat{\mathbf{q}}) \frac{(2\kappa)^{Z/\kappa}\Gamma(1+Z/\kappa)}{(q^2+\kappa^2)^{1+Z/\kappa}}, \tag{A4}$$

where ± 1 corresponds to $q\to\pm i\kappa$. For the l-values used in this work Eq. (A4) can be verified directly by calculating limits of the explicit representation of the relevant Gauss' hypergeometric functions from Eq. (A3) and substituting these expressions into the terms in Eq. (A2).

[1] P. B. Corkum, Phys. Rev. Lett. **71**, 1994 (1993).
[2] P. Agostini and L. F. DiMauro, Rep. Prog. Phys. **67**, 813 (2004).
[3] A. Scrinzi, M. Y. Ivanov, R. Kienberger, and D. M. Villeneuve, J. Phys. B **39**, R1 (2006).
[4] M. Lein, Phys. Rev. A **72**, 053816 (2005).
[5] D. A. Telnov and Shih-I Chu, Phys. Rev. A **71**, 013408 (2005).
[6] G. L. Kamta and A. D. Bandrauk, Phys. Rev. A **71**, 053407 (2005).
[7] X. X. Zhou, X. M. Tong, Z. X. Zhao, and C. D. Lin, Phys. Rev.

A **72**, 033412 (2005).
[8] B. Zimmermann, M. Lein, and J. M. Rost, Phys. Rev. A **71**, 033401 (2005).
[9] J. Itatani, J. Levesque, D. Zeidler, H. Niikura, H. Pépin, J. C. Kieffer, P. B. Corkum, and D. M. Villeneuve, Nature (London) **432**, 867 (2004).
[10] M. Lein, Phys. Rev. Lett. **94**, 053004 (2005).
[11] T. Kanai, S. Minemoto, and H. Sakai, Nature (London) **435**, 470 (2005).
[12] J. Itatani, D. Zeidler, J. Levesque, M. Spanner, D. M. Villeneuve, and P. B. Corkum, Phys. Rev. Lett. **94**, 123902 (2005).
[13] M. Lewenstein, P. Balcou, M. Y. Ivanov, A. L'Huillier, and P. B. Corkum, Phys. Rev. A **49**, 2117 (1994).
[14] C. C. Chirilă and M. Lein, Phys. Rev. A **73**, 023410 (2006).
[15] M. Y. Kuchiev and V. N. Ostrovsky, Phys. Rev. A **60**, 3111 (1999).
[16] T. K. Kjeldsen and L. B. Madsen, Phys. Rev. A **71**, 023411 (2005).
[17] E. U. Condon, Phys. Rev. **36**, 1121 (1930).
[18] V. N. Ostrovsky and J. B. Greenwood, J. Phys. B **38**, 1867 (2005).
[19] G. F. Gribakin and M. Y. Kuchiev, Phys. Rev. A **55**, 3760 (1997).
[20] V. N. Ostrovsky, J. Phys. B **38**, 4399 (2005).
[21] J. J. Sakurai, *Modern Quantum Mechanics*, revised ed. (Addison-Wesley, Reading, MA, 1994).
[22] J. Kobus, L. Laaksonen, and D. Sundholm, Comput. Phys. Commun. **98**, 346 (1996).
[23] J. Ortigoso, M. Rodríguez, M. Gupta, and B. Friedrich, J. Chem. Phys. **110**, 3870 (1999).
[24] *NIST Chemistry WebBook, NIST Standard Reference Database Number 69*, edited by P. Linstrom and W. Mallard (National Institute of Standards and Technology, Gaithersburg, MD 2005).
[25] R. Torres, R. de Nalda, and J. P. Marangos, Phys. Rev. A **72**, 023420 (2005).
[26] M. Halmann and I. Laulicht, J. Chem. Phys. **43**, 1503 (1965).
[27] R. W. Nicholls, J. Phys. B **1**, 1192 (1968).
[28] G. H. Dunn, J. Chem. Phys. **44**, 2592 (1966).
[29] S. Cohen, J. R. Hiskes, and R. J. Riddell, Jr., Phys. Rev. **119**, 1025 (1960).
[30] T. K. Kjeldsen and L. B. Madsen, J. Phys. B **37**, 2033 (2004).
[31] K. Miyazaki, M. Kaku, G. Miyaji, A. Abdurrouf, and F. H. M. Faisal, Phys. Rev. Lett. **95**, 243903 (2005).
[32] T. K. Kjeldsen and L. B. Madsen, Phys. Rev. Lett. **95**, 073004 (2005).
[33] L.-Y. Peng (private communication).
[34] M. Abramowitz and I. A. Stegun, *Handbook of Mathematical Functions With Fourmlas, Graphs, and Mathematical Tables* (U. S. Government Printing Office, Washington, DC, 1964).
[35] I. S. Gradshteyn and I. M. Ryzhik, *Table of Integrals, Series, and Products*, 4th ed. (Academic Press, New York, 1965).
[36] A. Gazibegović-Busuladžić, D. B. Milošević, and W. Becker, Phys. Rev. A **70**, 053403 (2004).